Chinese Chemical Letters 35 (2024) 108781

Contents lists available at ScienceDirect

Chinese Chemical Letters

journal homepage: www.elsevier.com/locate/cclet

Promoted NH_3-SCR activity and hydrothermal stability of Cu-SSZ-50 catalyst synthesized by one-pot method

Jinpeng Du[a,b], Jingyi Wang[a,c], Yulong Shan[d], Shichao Han[a,b], Wenpo Shan[a,b,*], Hong He[a,c,d,*]

[a] Center for Excellence in Regional Atmospheric Environment, Institute of Urban Environment, Chinese Academy of Sciences, Xiamen 361021, China
[b] Zhejiang Key Laboratory of Urban Environmental Processes and Pollution Control, Ningbo Urban Environment Observation and Research Station, Institute of Urban Environment, Chinese Academy of Sciences, Ningbo 315800, China
[c] University of Chinese Academy of Sciences, Beijing 100049, China
[d] State Key Joint Laboratory of Environment Simulation and Pollution Control, Research Center for Eco-Environmental Sciences, Chinese Academy of Sciences, Beijing 100085, China

ARTICLE INFO

Article history:
Received 8 February 2023
Revised 14 June 2023
Accepted 5 July 2023
Available online 6 July 2023

Keywords:
NH_3-SCR
Cu-SSZ-50
One-pot synthesis
Si/Al ratio
Cu species distribution
Reaction mechanism

ABSTRACT

Nitrogen oxide (NO_x) is one of the most critical contaminants in the air, and the control of NO_x emission from diesel vehicles is very important. Cu-based small-pore zeolites have already been applied for NO_x abatement on diesel vehicles. Among the small-pore zeolites, Cu-SSZ-50 catalysts with good NH_3-SCR catalytic activity were believed to have potential for application. In this study, a one-pot synthesis method for Cu-SSZ-50 catalysts was developed for the first time, using the co-templates of Cu-TEPA and 2,6-dimethyl-*N*-methylpyridinium hydroxide. In this synthesis method, Cu-SSZ-50 with various Cu contents can be obtained by adjusting the amount of Cu-TEPA without the need for a further after-treatment process. The addition of Cu-TEPA affected the framework atoms and Cu species, and a lower Si/Al ratio and more SCR active Cu species were obtained. The synthesized catalyst with a Cu/Al ratio of 0.40 exhibited over 90% NO_x conversion between 200 °C and 450 °C for the selective catalytic reduction of NO_x with NH_3 (NH_3-SCR). Meanwhile, over 80% NO_x conversion could be obtained from 250 °C to 450 °C after hydrothermal aging at 750 °C for 16 h. In addition, both L-H and E-R mechanisms were proven to exist for the one-pot-synthesized Cu-SSZ-50 by *in situ* DRIFTS experiments. The simple synthesis procedure, excellent catalytic activity and hydrothermal stability brighten the prospects for the application of Cu-SSZ-50.

Air pollution problems such as $PM_{2.5}$ and O_3 have become increasingly urgent environmental challenges. The control of NO_x, especially that emitted from diesel vehicles, is an effective way to realize co-control of $PM_{2.5}$ and O_3 pollution [1–4]. The NH_3-SCR device is applied in the after-treatment system of diesel vehicles for the abatement of NO_x. Among NH_3-SCR catalysts, Cu-based small-pore zeolites are known for their excellent catalytic activity and hydrothermal stability, with Cu-SSZ-13 realizing commercialization [5,6]. In addition to Cu-SSZ-13, some other Cu-based small-pore zeolites also have high potential for industrial application [7–11]. Cu-SSZ-50 with the RTH structure (Scheme S1 in Supporting information) has been demonstrated to perform well in NH_3-SCR [12,13]. There are two Cu^{2+} species existing in Cu-SSZ-50 zeolites: α Cu^{2+} species are more SCR-active and located near 8-membered rings (8mr), while β Cu^{2+} species located near rth cages are less SCR-active (Scheme S2 in Supporting information). Cu^{2+} species are preferentially located near rth cages; therefore, Cu-SSZ-50 catalysts present poor SCR activity when Cu loading is low. When the β Cu^{2+} location is occupied, more α Cu^{2+} species form, and Cu-SSZ-50 catalysts show high NO_x conversion with high Cu loading [14].

Although Cu-SSZ-50 with appropriate Cu loading possesses good NH_3-SCR activity, its weak hydrothermal stability casts a shadow on its application for diesel vehicles [12]. It was found that the accumulation of Cu ions was the main reason causing inactivation. However, higher Cu loading may hinder the migration of Cu ions; therefore, Cu-SSZ-50 catalysts with higher Cu/Al ratios showed better hydrothermal stability [14]. Thus, increasing the amount of active Cu ions and simultaneously avoiding the formation of a large amount of Cu_xO_y species may improve the hydrothermal stability of Cu-SSZ-50.

* Corresponding authors at: Center for Excellence in Regional Atmospheric Environment, Institute of Urban Environment, Chinese Academy of Sciences, Xiamen 361021, China.
E-mail addresses: wpshan@iue.ac.cn (W. Shan), honghe@rcees.ac.cn (H. He).

https://doi.org/10.1016/j.cclet.2023.108781
1001-8417/

The traditional methods for the synthesis of Cu-SSZ-50 require expensive templates and long crystallization times [15,16]. Xu *et al.* used 2,6-dimethyl-*N*-methylpyridinium as a template and obtained RTH zeolite in 12 h, which improved the application prospects of Cu-SSZ-50 [17]. However, several ion-exchange processes are still needed to obtain Cu-SSZ-50 catalysts. Ren *et al.* first invented the one-pot synthesis of Cu-SSZ-13 with Cu-TEPA as the only template [18,19]. However, the Cu content of the Cu-SSZ-13 synthesized by this method is rather high, and post-treatment processes are needed to obtain better catalytic performance. Subsequently, Corma *et al.* utilized TMAda and Cu-TEPA as co-templates to synthesize Cu-SSZ-13 with controllable Cu content [20]. In addition to Cu-SSZ-13, the one-pot synthesis of Cu-SAPO-34 and Cu-SSZ-39 have also been accomplished by Corma *et al.*, following the co-template strategy [21,22]. Inspired by these studies, the one-pot synthesis of Cu-SSZ-50 using 2,6-dimethyl-*N*-methylpyridinium hydroxide and Cu-TEPA as co-templates was conducted in this study. Furthermore, in the synthesis of Cu-SSZ-13, the molecular size of TEPA is smaller than the traditional template TMAdaOH; therefore, Na^+ ions occupy the free space, resulting in a lower Si/Al ratio [18,19]. A lower Si/Al ratio creates more ion-exchange sites for Cu species, which may hinder the mobility of Cu^{2+} ions. Therefore, introducing Cu-TEPA as the co-template may help to decrease the Si/Al ratio of Cu-SSZ-50, while also improving the hydrothermal stability.

In this study, to optimize the synthesis process and catalytic performance of Cu-SSZ-50 catalysts, the one-pot synthesis method was developed. By changing the amount of Cu-TEPA, Cu-SSZ-50 catalysts with various Cu/Al ratios were obtained without the need for a further after-treatment process. The obtained Cu-SSZ-50 catalysts with various Cu/Al ratios were tested for their NH_3-SCR performance and characterized by various methods, including XRD, SEM, NMR, ICP-OES, EPR, H_2-TPR, and NH_3-TPD. Furthermore, the catalytic activity and hydrothermal stability of one-pot-synthesized and ion-exchanged Cu-SSZ-50 catalysts with similar Cu/Al ratios were compared. Finally, the NH_3-SCR reaction mechanism of the one-pot synthesized Cu-SSZ-50 was investigated by *in situ* DRIFTS experiments.

The XRD patterns of the one-pot-synthesized Cu-SSZ-50 catalysts are shown in Fig. 1a. All the Cu-SSZ-50 catalysts with various Cu/Al ratios showed the RTH structure with good crystallization. However, the crystallinity of OP-0.40 was a little lower than that of the other catalysts, and the diffraction peak of CuO (38.7°) was observed in the pattern. The XRD patterns of the hydrothermally aged Cu-SSZ-50 samples prepared by one-pot synthesis and

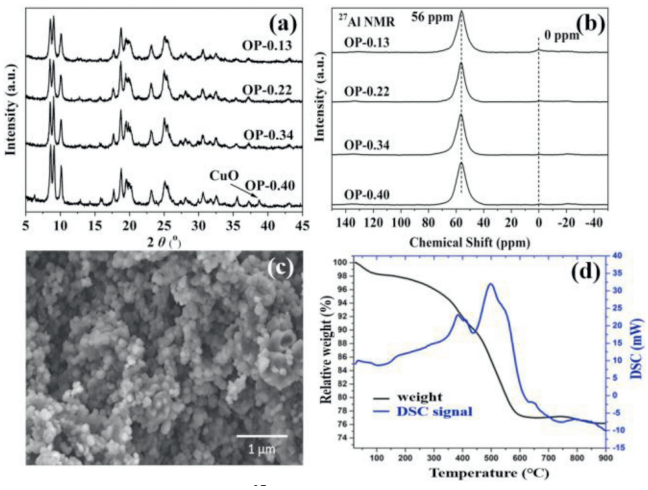

Fig. 1. (a) XRD patterns, (b) ^{27}Al NMR, (c) SEM images, (d) TG-DSC curves of the one-pot-synthesized Cu-SSZ-50 catalysts.

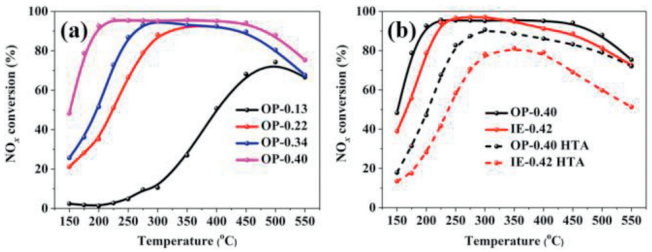

Fig. 2. (a) NH_3-SCR activity results for the one-pot-synthesized Cu-SSZ-50 catalysts; (b) Catalytic activity and hydrothermal stability results of OP-0.40 and IE-0.42.

ion-exchange methods are presented in Fig. S1 (Supporting information). After hydrothermal aging at 750 °C for 16 h, both OP-0.40 HTA and IE-0.42 HTA kept the RTH structure with good crystallization. A characteristic diffraction peak of CuO (38.7°) was observed for OP-0.40 HTA but not IE-0.42 HTA [23].

^{27}Al NMR spectra were utilized to investigate the coordination environment of Al atoms in the prepared catalysts, and the spectra are presented in Fig. 1b. The peaks at chemical shifts of 56 ppm and 0 ppm are assigned to the tetrahedral and octahedral Al atoms, respectively [24]. Only a weak peak at 0 ppm corresponding to extra-framework Al atoms can be observed in the spectrum of OP-0.13, and no peak at 0 ppm emerged for OP-0.22, OP-0.34 or OP-0.40 [25]. This result was in accordance with the XRD results showing that the one-pot-synthesized Cu-SSZ-50 catalysts were well-crystallized.

The SEM image of OP-0.40 presented in Fig. 1c shows that it consists of particles around 200 nm in size with relatively uniform shape. The SEM images of the catalysts with other Cu/Al ratios are presented in Fig. S2 (Supporting information), and they also present uniform shapes. Compared with the previously reported conventional SSZ-50, the particle sizes of the one-pot-synthesized Cu-SSZ-50 catalysts were not quite as uniform [13]. This result indicates that Cu-TEPA can influence the morphology of Cu-SSZ-50, although the particles were still in a cubic form.

The elemental compositions of the catalysts are summarized in Table S1 (Supporting information), according to the results of ICP-OES. Compared with IE-0.42, more Na^+ ions existed in the one-pot-synthesized catalysts. This is because three ion-exchange processes were conducted to obtain IE-0.42, while no aftertreatment process was carried out for the one-pot-synthesized catalysts. Furthermore, the Si/Al ratios of the one-pot-synthesized catalysts were similar to that of IE-0.42, except for OP-0.40. The Si/Al ratio of OP-0.40 was relatively low among the prepared catalysts, probably due to the addition of abundant Cu-TEPA, resulting in higher Cu content compared with the IE-0.42 sample of similar Cu/Al ratio.

TG-DSC was used to investigate the weight changes of the catalysts as a function of temperature, with all samples being derived from the initial products without any calcination. The TG and DSC curves for the conventional SSZ-50 sample are presented in Fig. S3 (Supporting information). A major exothermic peak emerged at around 600 °C with a weight loss of about 15%, indicating the decomposition of the sole template (2,6-dimethyl-*N*-methylpyridinium hydroxide) [13]. Meanwhile, the curves for the one-pot-synthesized Cu-SSZ-50 are shown in Fig. 1d. Two major exothermic peaks appeared around 400 °C and 550 °C, with a total weight loss of about 25%. According to the results in Fig. S3 and previous reports, these two exothermic peaks were assigned to the decomposition of TEPA (400 °C) and 2,6-dimethyl-*N*-methylpyridinium hydroxide (550 °C), respectively [13,18,19].

NH_3-SCR activity tests were carried out for the Cu-SSZ-50 catalysts, and the results are shown in Fig. 2. For the one-pot-synthesized catalysts, NO_x conversion improved with increasing Cu/Al ratio over the whole temperature range. This phenomenon

indicated that Cu ions can deposit in the active sites of Cu-SSZ-50 with only a small amount accumulating outside the cavities. A decrease in NO_x conversion was observed over 500 °C for all the catalysts, which could be due to the presence of some Cu_xO_y species facilitating NH_3 oxidation. A dramatic increase in catalytic activity was seen when Cu/Al increased from 0.13 to 0.22. A similar phenomenon was also observed in the conventional Cu-SSZ-50 catalysts previously reported by our group [14]. The OP-0.40 sample showed the best catalytic performance, with over 90% NO_x conversion obtained from 200 °C to 450 °C. Therefore, the hydrothermal stability of OP-0.40 was further tested and compared with that of the ion-exchanged Cu-SSZ-50 catalyst with similar Cu/Al ratio. For the fresh catalysts, OP-0.40 presented better catalytic activity in both the low- and high-temperature ranges. After hydrothermal treatment, the gap between the NO_x conversion of OP-0.40 HTA and IE-0.42 HTA became even larger, and over 80% NO_x conversion could be obtained from 250 °C to 450 °C for OP-0.40 HTA. The N_2O concentrations and N_2 selectivity of the prepared catalysts during NH_3-SCR activity test were shown in Fig. S4 (Supporting information). Compared with IE-0.42 and IE-0.42-HTA, more N_2O was emitted for OP-0.40 and OP-0.40-HTA, respectively. Nevertheless, less than 15 ppm of N_2O and over 96% N_2 selectivity was obtained for all the catalysts at the tested temperatures, indicating that the prepared catalysts possessed high N_2 selectivity.

An NH_3 oxidation test was carried out for OP-0.40 and IE-0.42, and the results are presented in Fig. S5 (Supporting information). IE-0.42 presented higher NH_3 oxidation conversion than OP-0.40 over 350 °C, which explained why OP-0.40 possessed better NH_3-SCR activity than IE-0.42 at high temperature. A SO_2 resistance test was also conducted for OP-0.40 and IE-0.42, with the results being shown in Fig. S6 (Supporting information). Nearly 100% NO_x conversion was obtained with OP-0.40 and IE-0.42 at 250 °C. When 50 ppm SO_2 was introduced, a dramatic decrease in NO_x conversion can be seen for both catalysts. IE-0.42 possessed higher NO_x conversion than OP-0.40 before 80 min, while the NO_x conversion over OP-0.40 was a little higher after that. When SO_2 was cut off, the NO_x conversion for OP-0.40 and IE-0.42 did not increase significantly. However, after regeneration at 600 °C, NO_x conversion was recovered to the level observed under fresh conditions for both catalysts. The results indicated the SCR activity of Cu-SSZ-50 catalysts was significantly affected by SO_2; meanwhile, regeneration was an effective way to recover activity.

EPR experiments were carried out to investigate the coordination environment of Cu^{2+} ions, with the spectra shown in Fig. 3. All the tested catalysts presented fourfold split hyperfine spectra with $g_{II} = 2.37$ and $A_{II} = 140$ G, which further proved that Cu^{2+} ions can be deposited at "ion-exchange sites" [26,27]. To quantify the amount of Cu ions, the relative Cu contents of the catalysts were calculated by quadratic integration of the EPR signals, and the results are presented in Fig. S7 (Supporting information). The relative Cu contents of the one-pot-synthesized Cu-SSZ-50 catalysts increased with the Cu/Al ratio. The trend of the EPR signals for the

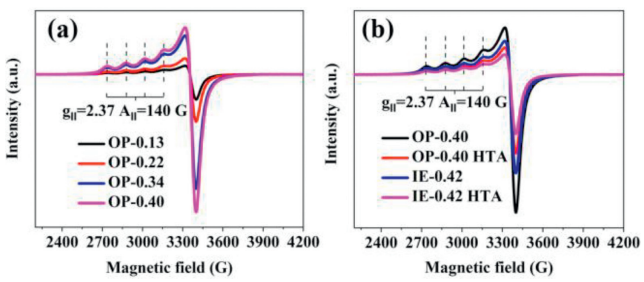

Fig. 3. EPR spectra of (a) one-pot-synthesized Cu-SSZ-50 catalysts, (b) fresh and hydrothermally aged OP-0.40 and IE-0.42.

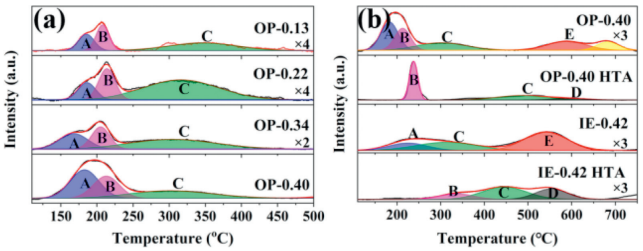

Fig. 4. H_2-TPR profiles of (a) one-pot-synthesized Cu-SSZ-50 catalysts, (b) fresh and hydrothermally aged OP-0.40 and IE-0.42.

one-pot-synthesized Cu-SSZ-50 was in accordance with the ICP results. In Fig. 3b, the EPR results of OP-0.40 and IE-0.42 before and after hydrothermal aging are compared. The relative Cu contents followed the order OP-0.40 > IE-0.42 > OP-0.40 HTA > IE-0.42 HTA. Although the Cu/Al ratios of OP-0.40 and IE-0.42 were similar, the EPR-active Cu^{2+} ions of these two catalysts were clearly different. As the ICP results showed, the Si/Al ratio of OP-0.40 was lower than that of IE-0.42, indicating the presence of more electronic defects in OP-0.40 for the deposition of Cu^{2+} ions. Therefore, OP-0.40 showed better catalytic activity than IE-0.42, as illustrated in Fig. 2b. Furthermore, after hydrothermal aging, a dramatic decrease in the amount of Cu^{2+} ions was observed in the EPR spectra for both OP-0.40 HTA and IE-0.42 HTA (Fig. 3b and Fig. S7), inducing a decrease in NO_x conversion for both catalysts (Fig. 2b). More Cu^{2+} ions were obtained in OP-0.40 HTA than IE-0.42 HTA; thus, OP-0.40 HTA performed better in the NH_3-SCR test.

H_2-TPR experiments were carried out to investigate the redox ability of the prepared catalysts as well to help distinguish the Cu species, with the profiles displayed in Fig. 4. Shan *et al.* thoroughly investigated the species of Cu^{2+} ions in RTH zeolites, and two kinds of Cu^{2+} ions were proposed, named α- and β-Cu ions. α Cu ions were located at relatively unstable sites where Cu^{2+} ions are more easily reduced, while β-Cu ions occupied relatively stable sites with lower redox ability [14]. The proposed locations of the two Cu^{2+} species are illustrated in Scheme S2; however, precise identification of the Cu^{2+} ions sites will require further investigation. For all the prepared catalysts, peak A was assigned to α-Cu ions ($Cu(OH)^+$), peak B was attributed to Cu_xO_y species, and peak C to the reduction of β-Cu ions (Cu^{2+}) [14]. As can be seen, most of the Cu species were in the form of Cu ions, and only a small amount of Cu_xO_y species existed, confirming that the formation of active Cu^{2+} ions is dominant in the one-pot synthesis. According to the peak areas, the relative contents of the two Cu ions and Cu_xO_y species in the samples are summarized in Fig. S8 (Supporting information). For the one-pot-synthesized catalysts, both α- and β-Cu ions existed regardless of the Cu/Al ratio; however, α-Cu ions did not form until the Cu/Al ratio increased to 0.27 in the conventional Cu-SSZ-50 catalysts [14]. Furthermore, the amounts of both α- and β-Cu ions increased with the increase in the Cu/Al ratio, leading to improvement of the NH_3-SCR performance of the one-pot-synthesized catalysts, as illustrated in Fig. 2a. The relative contents of Cu_xO_y species are also summarized in Fig. S8, and Cu_xO_y species can be observed in all the catalysts, accounting for the decrease in NO_x conversion above 500 °C. Although OP-0.40 HTA possessed more Cu_xO_y species than IE-0.42 HTA, OP-0.40 HTA still performed better in the NH_3-SCR reaction. The H_2-TPR profiles of OP-0.40 and IE-0.42 before and after hydrothermal aging are compared in Fig. 4b. The peaks above 500 °C for OP-0.40 were assigned to the reduction of Cu^+ to Cu^0, and the peak D for the aged catalysts was attributed to $CuAlO_x$ species [28–30]. As can be seen in Fig. 4b and Fig. S8, the α-Cu ions disappeared after hydrothermal aging, and some of them transformed into β-Cu ions, indicating that α-Cu ions are unstable in the catalyst. The same phenomenon can

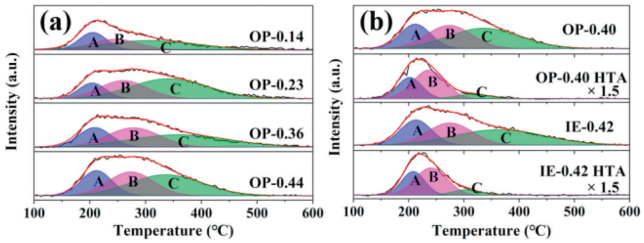

Fig. 5. NH_3-TPD profiles of (a) one-pot-synthesized Cu-SSZ-50 catalysts, (b) fresh and hydrothermally aged OP-0.40 and IE-0.42.

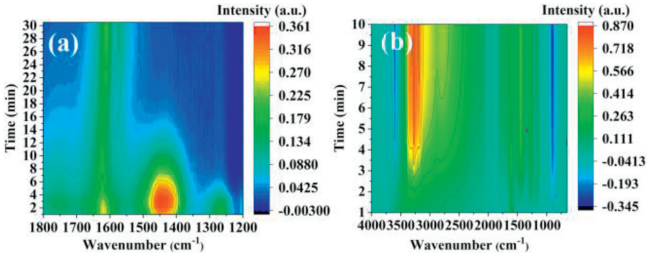

Fig. 6. Color images of *in situ* DRIFTS spectra of (a) adsorbed NH_3 and $NO+O_2$ on OP-0.40, (b) adsorbed $NO+O_2$ and NH_3 on OP-0.40.

be observed in Fig. S9 (Supporting information), where α-Cu ions transformed into β-Cu ions. On the other hand, more β-Cu ions were maintained in OP-0.40 HTA after hydrothermal aging compared to IE-0.42 HTA, which was in accordance with the EPR results and can explain the better hydrothermal stability of OP-0.40.

NH_3-TPD was used to investigate the acidity of the prepared catalysts, and the profiles are shown in Fig. 5, with the acidity summarized in Fig. S10 (Supporting information). Peak A was assigned to weak acid sites mainly from terminal hydroxyl species or physically adsorbed NH_3; peak B was attributed to medium acid sites, which are Lewis acid sites (Cu^{2+}); and peak C corresponded to strong acid sites from Brønsted acid sites (Al-OH-Si) [24,31]. For the one-pot-synthesized Cu-SSZ-50 catalysts, the total amount of acid sites increased with the Cu/Al ratio. Meanwhile, the amount of Lewis acid sites (Cu^{2+}) also rose with the increase in Cu/Al ratios, which was in accordance with the results of EPR and H_2-TPR. Acid sites, especially Lewis acid sites, are critical for the NH_3-SCR reaction; thus, the results of NH_3-TPD partially explained the trends of catalytic activity for the one-pot-synthesized Cu-SSZ-50. In addition, OP-0.40 and IE-0.42 possessed similar amounts of acid sites of each type. It is worth mentioning that compared with OP-0.40 and IE-0.42, the peak area of B (Lewis acid sites) for OP-0.40 HTA and IE-0.42 HTA increased; meanwhile, the peak area of C (Brønsted acid sites) decreased dramatically. *In situ* DRIFTS of NH_3 absorbance experiments were also carried out to detect the amount and intensity of acid sites. As presented in Fig. S11 (Supporting information), the peak at 1650∼1600 cm^{-1} was attributed to Lewis acid sites (Cu^{2+} species), and the peak around 1500∼1450 cm^{-1} was assigned to Brønsted acid sites (framework Al-OH). After hydrothermal aging, the intensity of peaks associated with Lewis acid sites increased and those of Brønsted acid sites decreased. A similar phenomenon was also observed in the study of Cu-SSZ-13. $Cu(OH)^+$ species can transform into Cu species with the consumption of Brønsted acid sites during the hydrothermal aging process of Cu-SSZ-13, following the equation: $Cu(OH)^+ + H^+ = Cu^{2+} + H_2O$. More NH_3 molecules can be absorbed on Cu^{2+} species than $Cu(OH)^+$ species; thus, the desorption of NH_3 on Lewis acid sites increased [32,33]. In this study, some α-Cu ions transformed into β-Cu ions during the hydrothermal aging process, as presented in the H_2-TPR results. α-Cu ions with better redox ability were in the form of $ZCu(OH)^+$, and β-Cu ions were in the form of Cu^{2+}. Therefore, the desorption of NH_3 from Lewis acid sites increased and the desorption of NH_3 from Brønsted acid sites decreased after hydrothermal aging of both OP-0.40 HTA and IE-0.42 HTA.

To investigate the NH_3-SCR reaction process on the OP-0.40 catalyst, *in situ* DRIFTS experiments were carried out, and the results are presented in Fig. 6 and Fig. S12 (Supporting information). As presented in Fig. S12, the negative peaks at 3725 and 3599 cm^{-1} were attributed to the consumption of OH from Brønsted acid sites by NH_3. The peaks at 3333, 3275 and 3187 cm^{-1} were assigned to the stretching vibration of N-H from NH_4^+ species. The peaks at 1621 and 1451 cm^{-1} corresponded to the bending vibration of N-H bonds from the adsorption of NH_3 on Lewis acid sites and Brønsted acid sites, respectively [34,35]. Meanwhile, the negative peaks at 937 and 904 cm^{-1} were related to the release of α and β Cu^{2+} ions, which disturbed the skeleton T-O-T vibration by the coordination of Cu ions and NH_3 [18]. Furthermore, after the introduction of NO and O_2, the peaks appearing at 1609 and 1574 cm^{-1} were attributed to bridging nitrate species and bidentate nitrate species, respectively [36,37].

First, the reaction of adsorbed NH_3 and $NO+O_2$ was investigated, and color images of the *in situ* DRIFTS spectra are presented in Fig. 6a. When NO and O_2 were introduced, NH_3 adsorbed at Lewis acid sites (around 1621 cm^{-1}) began to be consumed quickly. In the first 4 min, the peak around 1621 cm^{-1} decreased noticeably; however, due to the interference of nitrate species, this peak began to increase from the 6th min. Meanwhile, the consumption of NH_3 adsorbed at Brønsted acid sites (around 1451 cm^{-1}) was much slower, and the peak did not even decrease until the 4th min. The results above indicated that NH_3 adsorbed at Lewis acid sites reacted with $NO+O_2$ predominantly, following the E-R mechanism, while the NH_3 adsorbed at Brønsted acid sites mainly played a complementary role.

Furthermore, the reaction processes of nitrate species and NH_3 were investigated. Due to interference from NH_3 adsorption peaks, the consumption of nitrate species cannot be seen in Fig. 6b. However, the peak change can be observed in Fig. S12b. With the introduction of NH_3, the peaks at 1609 and 1574 cm^{-1} decreased simultaneously in the first several minutes. Due to the adsorption of NH_3, the peak around 1621 cm^{-1} began to increase from the 5^{th} min, interfering with the peak intensity at 1609 cm^{-1}. The peak at 1574 cm^{-1} diminished from the 5^{th} min, indicating that nitrate species were consumed in the first 5 min. The results above indicated that the nitrate species could react with NH_3, following the L-H mechanism. Therefore, both the E-R mechanism and L-H mechanism existed on OP-0.40 during the NH_3-SCR reaction process [38,39].

In this study, Cu-SSZ-50 catalysts were one-pot-synthesized using 2,6-dimethyl-*N*-methylpyridinium hydroxide and Cu-TEPA as co-templates. By changing the amount of Cu-TEPA, catalysts of various Cu/Al ratios with good crystallinity were obtained without further after-treatment. More importantly, the Cu^{2+} ions were predominantly deposited at active sites, despite the existence of a small amount of Cu_xO_y species. In the conventional ion-exchanged Cu-SSZ-50 catalysts, only β-Cu species existed when the Cu loading was low (<1.4 wt%) [14]. However, both α- and β-Cu species existed in the one-pot-synthesized Cu-SSZ-50, regardless of the Cu/Al ratio. For one thing, abundant retained Na^+ ions occupied the stable ion-exchange sites, which increased the difficulty of forming β-Cu species. For another, Cu-TEPA molecules were able to be accommodated in large cages initially, increasing the possibility of the formation of α-Cu species. Cu_xO_y species formed easily in the one-pot-synthesized Cu-SSZ-50 catalysts, as illustrated by H_2-TPR results. However, OP-0.40 still possessed better catalytic activity than IE-0.42 even in the high-temperature range, indicating

that the existence of Cu_xO_y species did not cause a dramatic decrease in NO_x conversion.

The poor hydrothermal stability of Cu-SSZ-50 zeolites is a roadblock for their application in NO_x abatement on diesel vehicles [12,14]. The RTH structure can endure the effects of steam up to 900 °C for 8 h, and the deactivation of Cu-SSZ-50 after hydrothermal aging at 750 °C for 16 h was mainly due to the loss of Cu^{2+} ions [14,16]. The conclusion was drawn from our previous study that Cu-SSZ-50 catalysts with higher Cu/Al ratios possessed better hydrothermal stability [14]. It is worth noting that too much Cu-TEPA in the initial synthesis gel can influence the crystallization of Cu-SSZ-50; thus, the highest Cu/Al of the one-pot synthesized Cu-SSZ-50 catalyst was only 0.40. OP-0.40, with the largest amount of Cu-TEPA in the initial synthesis gel, could easily form more framework Al atoms, resulting in its relatively low Si/Al ratio compared to IE-0.42. Therefore, compared with IE-0.42, more Cu^{2+} ions existed in OP-0.40 owing to the lower Si/Al ratio. Higher Cu loading hinders the migration of Cu^{2+} ions; thus, more Cu^{2+} ions remained in OP-0.40 HTA. Therefore, OP-0.40 HTA possessed better NH_3-SCR activity than IE-0.42 HTA.

In conclusion, Cu-SSZ-50 catalysts with various Cu contents were produced *via* a one-pot synthesis method. All the one-pot-synthesized Cu-SSZ-50 catalysts were well-crystallized with hardly any extra-framework Al atoms. Both α- and β-Cu^{2+} species existed in the one-pot-synthesized Cu-SSZ-50 catalysts with a small portion of Cu_xO_y species formed regardless of Cu content. Owing to the addition of Cu-TEPA, a lower Si/Al ratio was obtained in OP-0.40, and this catalyst possessed more active Cu^{2+} ions than IE-0.42. Higher Cu loading in OP-0.40 limited the Cu^{2+} ions' mobility; therefore, it showed good hydrothermal stability. Furthermore, both the L-H and E-R mechanisms were observed in the NH_3-SCR reaction process in OP-0.40.

Declaration of competing interest

The authors declare that they have no known competing financial interests or personal relationships that could have appeared to influence the work reported in this paper.

Acknowledgments

This work was financially supported by the National Natural Science Foundation of China (Nos. 52200136, 52225004 and 51978640) and the Science and Technology Innovation "2025" major program in Ningbo (No. 2020Z103)

Supplementary materials

Supplementary material associated with this article can be found, in the online version, at doi:10.1016/j.cclet.2023.108781.

References

[1] D. Ding, J. Xing, S. Wang, et al., Environ. Sci. Technol. 56 (2022) 739–749.
[2] Y. Tan, P. Henderick, S. Yoon, et al., Environ. Sci. Technol. 53 (2019) 5504–5511.
[3] S. Jiang, T. Li, J. Zheng, et al., Environ. Sci. Technol. 54 (2020) 14740–14749.
[4] P. Li, Y. Xin, Q. Li, et al., Environ. Sci. Technol. 46 (2012) 9600–9605.
[5] J.H. Kwak, D. Tran, J. Szanyi, C.H.F. Peden, J.H. Lee, Catal. Lett. 164 (2012) 295–301.
[6] D.W. Fickel, E. D'Addio, J.A. Lauterbach, R.F. Lobo, Appl. Catal. B: Environ. 102 (2011) 441–448.
[7] M. Moliner, C. Franch, E. Palomares, M. Grill, A. Corma, Chem. Commun. 48 (2012) 8264–8266.
[8] H. Wang, R. Xu, Y. Jin, R. Zhang, Catal. Today 327 (2019) 295–307.
[9] J. Kim, S.J. Cho, D.H. Kim, ACS Catal. 7 (2017) 6070–6081.
[10] D. Jo, T. Ryu, G.T. Park, et al., ACS Catal. 6 (2016) 2443–2447.
[11] S. Zhang, S. Ming, L. Guo, et al., J. Hazard. Mater. 414 (2021) 125543–125554.
[12] J.D. Albarracin-Caballero, I. Khurana, J.R. Di Iorio, et al., React. Chem. Eng. 2 (2017) 168–179.
[13] H. Xu, Q. Wu, Y. Chu, et al., J. Mater. Chem. A 6 (2018) 8705–8711.
[14] Y. Shan, X. Shi, J. Du, Y. Yu, H. He, Catal. Sci. Technol. 9 (2019) 106–115.
[15] G.S. Lee, S.I. Zones, J. Solid State Chem. 167 (2002) 289–298.
[16] J.E. Schmidt, M.A. Deimund, D. Xie, M.E. Davis, Chem. Mater. 27 (2015) 3756–3762.
[17] H. Xu, W. Chen, Q. Wu, et al., J. Mater. Chem. A 7 (2019) 4420–4425.
[18] L. Ren, L. Zhu, C. Yang, et al., Chem. Commun. 47 (2011) 9789–9791.
[19] L. Ren, Y. Zhang, S. Zeng, et al., Chin. J. Catal. 33 (2012) 92–105.
[20] R. Martínez-Franco, M. Moliner, J.R. Thogersen, A. Corma, ChemCatChem 5 (2013) 3316–3323.
[21] R. Martínez-Franco, M. Moliner, C. Franch, A. Kustov, A. Corma, Appl. Catal. B: Environ. 127 (2012) 273–280.
[22] N. Martin, C.R. Boruntea, M. Moliner, A. Corma, Chem. Commun. 51 (2015) 11030–11033.
[23] B. Chen, R. Xu, R. Zhang, N. Liu, Environ. Sci. Technol. 48 (2014) 13909–13916.
[24] J. Liang, Y. Mi, G. Song, et al., J. Hazard. Mater. 398 (2020) 122986–122997.
[25] Y. Ma, S. Cheng, L. Cao, et al., Appl. Catal. A Gen. 602 (2020) 117650–117661.
[26] Y.J. Kim, J.K. Lee, K.M. Min, et al., J. Catal. 311 (2014) 447–457.
[27] Y. Zhang, Y. Wu, Y. Peng, et al., J. Phys. Chem. C 124 (2020) 28061–28073.
[28] Z. Chen, C. Fan, L. Pang, et al., Appl. Catal. B: Environ. 237 (2018) 116–127.
[29] Z. Zhao, R. Yu, R. Zhao, et al., Appl. Catal. B: Environ. 217 (2017) 421–428.
[30] W. Su, Z. Li, Y. Peng, J. Li, Phys. Chem. Chem. Phys. 17 (2015) 29142–29149.
[31] H. Tian, Y. Ping, Y. Zhang, et al., J. Hazard. Mater. 416 (2021) 126194–126203.
[32] J. Luo, F. Gao, K. Kamasamudram, et al., J. Catal. 348 (2017) 291–299.
[33] J. Luo, K. Kamasamudram, N. Currier, A. Yezerets, Eng. Sci. 190 (2018) 60–67.
[34] S. Han, J. Cheng, C. Zheng, et al., Appl. Surf. Sci. 419 (2017) 382–392.
[35] S. Han, Q. Ye, S. Cheng, T. Kang, H. Dai, Catal. Sci. Technol. 7 (2017) 703–717.
[36] N. Zhu, Y. Shan, W. Shan, et al., Environ. Sci. Technol. 54 (2020) 15499–15506.
[37] M.P. Ruggeri, I. Nova, E. Tronconi, et al., Appl. Catal. B: Environ. 166-167 (2015) 181–192.
[38] N. Zhu, Y. Shan, W. Shan, et al., Environ. Sci. Technol. 55 (2021) 16175–16183.
[39] J. Du, Y. Shan, Y. Sun, et al., Appl. Catal. B: Environ. 294 (2021) 120237–120246.